**O.Schennach, R.Pecnik, J.Woisetschläger, E.Göttlich, A.Marn, F.Heitmeir** (2007) *Influence of vane clocking on the unsteady flowfield in a one and a half stage transonic turbine*, Proc. 7th European Conference on Turbomachinery, 5-9 March 2007, Athens, pp 1259-1272

# INFLUENCE OF VANE CLOCKING ON THE UNSTEADY FLOWFIELD IN A ONE AND A HALF STAGE TRANSONIC TURBINE

*O. Schennach, R. Pecnik, J. Woisetschläger, E. Göttlich, A. Marn and F. Heitmeir*

Institute for Thermal Turbomachinery and Machine Dynamics
Graz University of Technology, Austria
oliver.schennach@tugraz.at
jakob.woisetschlaeger@tugraz.at

## ABSTRACT

**The current paper presents the results of numerical clocking investigations performed in a high-pressure transonic turbine with a downstream vane row (1.5 stage machine). A transient 3D-Navier Stokes calculation was done for four clocking positions and the three dimensional results are compared with Laser-Doppler-Velocimetry measurements at midspan. Two selected clocking positions are discussed in detail with the focus onto the midspan. Close to the leading edge of the second vane a significant change in shock strength is observed for different clocking positions.**

## NOMENCLATURE

| **Latin** | | | **Superscripts** | |
|---|---|---|---|---|
| $t$ | [s] | time | $\bar{}$ | ensemble-averaged properties |
| $\mathbf{V}$ | [m/s] | velocity vector | $=$ | time-averaged properties |
| $u, v$ | [m/s] | velocity components | $\sim$ | periodic quantity |
| $x, y, z$ | [m] | Cartesian coordinates | $'$ | unresolved fluctuating quantity |
| **Greek** | | | **Abbreviations** | |
| $\tau$ | [s] | blade passing period | CP | clocking position |
| **Subscripts** | | | LDV | Laser-Doppler-Velocimetry |
| $A$ | | first vane inlet | HP, LP | high pressure, low pressure |
| $C$ | | rotor outlet | PS | pressure surface |
| $D1, D3$ | | second vane outlet | SS | suction surface |

## INTRODUCTION

To meet the objective of reduced costs and more compactness of turbomachinery it is advantageous to reduce the number of stages resulting in high-pressure ratios and transonic conditions for these stages. To keep the efficiency at a high level a detailed understanding of the unsteady flow is necessary. The flow unsteadiness in turbomachinery is highly related to the vane-rotor motion and the wake-wake interaction. Additionally, in HP low aspect ratio turbines the secondary flows, strong potential fields and trailing edge shocks must be taken into account. These effects cause a time-varying, non-uniform flow field downstream of the stage affecting the performance and boundary layer development of the next vane row (Miller et al., 2003a, Tiedemann and Kost, 2001 and König et al., 2004.

Hummel (2002) performed a two dimensional numerical simulation of a one stage HP turbine and provided a guideline for positioning a second vane row in order to minimize the effect of the trailing edge shock strength onto the second vane.

The basic idea of clocking (also known as indexing) is to improve the overall efficiency by varying the circumferential and/or the axial position of adjacent vanes or blades. The most common method is to rotate the nozzle ring with respect to a downstream vane row, while the largest efficiency increase is achieved with equal blade counts. It is well known that a maximum of efficiency is achieved when the wake of the first vane impinges onto the leading edges of the second vanes.

Much research work has been performed to investigate the influence of clocking in subsonic turbines. Experimental results reported by Huber et al. (1996) for a two stage turbine showed a 0.8% efficiency variation in midspan due to clocking of the second stage vane. Time accurate numerical studies by Arnone et al. (2002) in a three stage LP turbine showed a 0.7% efficiency variation due clocking. Furthermore, investigations with different Reynolds numbers showed no major difference in the results. Reinmöller et al. (2002) investigated the influence of clocking on the flow field between rotor and second vane as well as downstream the second vane using hot wire probes and pneumatic probes supported by numerical simulations. The authors found 1% relative efficiency variation at midspan.

Recent research work focuses on clocking effects in transonic turbines. Billiard et al. (2005) focused on the heat transfer on the second vane in a 1.5 stage HP turbine. It was found that clocking changes the mean levels of the heat transfer as well as the intensity and the trajectory of the fluctuations. Gadea et al. (2004) investigated the influence of clocking onto the time resolved pressure field of a second vane tested in a 1.5 stage HP turbine. With the result that the optimum clocking position for aerodynamics is not the optimum for minimum unsteady forces. Haldemann et al. (2004) performed aerodynamic measurements in 1.5 stage HP turbine indicating an overall efficiency increase of about 2-3% using a variety of independent methods.

The current paper focuses on the propagation of shock waves at midspan of a highly loaded low aspect ratio transonic turbine stage with respect to two different clocking positions. An unsteady three dimensional Navier-Stokes calculation was performed to discuss the interaction mechanism in detail. Four circumferential measurement lines (gained with LDV) are used to validate the prediction. The experimental investigations were performed under engine representative conditions in a continuously running cold-flow test facility of the institute. Using non-intrusive optical measurement techniques such as LDV enables measurements close to the vane or blades and detects the interaction mechanisms.

## TEST FACILITY

The transonic test turbine of the Institute for Thermal Turbomachinery and Machine Dynamics is a continuously operating cold-flow open-circuit facility, which allows the testing of turbine stages with a diameter up to 800 mm in full flow similarity (corrected speed and pressure ratio). The turbine is driven by pressurized air, which is delivered by a separate 3 MW compressor station. A brake compressor delivers additional air mixed to the flow from the compressor station and increases the overall mass flow. The air temperature in the mixing chamber (turbine stage inlet) can be adjusted by coolers between 40 °C to 185 °C. The maximum shaft speed of the test rig is limited to 11550 rpm. Depending on the stage characteristic a maximum coupling power of 2.8 MW at a total mass flow of 22 kg/s can be reached. Detailed information on the design and construction of the facility can be found in Erhard and Gehrer (2000), on the operation in Neumayer et al. (2001).

### Turbine Stage tested

The meridional section of the turbine stage is given in Fig. 1. To provide access for all types of optical measurements the hub contour is cylindrical while the shroud contour is conical in the rotor

section. The second vane has a simple cylindrical contour and is designed as a low-pressure vane to prevent condensation of the humid air. Downstream of the second vane row a deswirler takes out the circumferential velocity and reduces flow velocity and therefore exhaust-losses (not shown in Fig. 1).

The optical access is realized with two glass windows downstream and upstream of the second vane row. The gap between rotor blade tip and casing as well as the clearance of the second vane to the hub are 1 mm. To allow a rotor-phase-resolved analysis of the measured velocities a reference signal provided by the monitoring system of the turbine was used to trigger the data sampling (uncertainty: blade pitch/300, a phase delay depending on speed was accounted for).

Some important operating conditions for this investigation and the geometrical data of the stage are given in Table 1.

**Laser-Doppler-Velocimetry**

The velocity measurement in the flow-field was performed by a two-component LDV-system. A detailed description of the optical setup is described in Schennach et al. (2006). The seeding particles used (nominal diameter of 0.3 µm) for the optical measurements guarantee sufficiently high particle response at transonic flow conditions.

**Table 1: Stage geometrical data and operating conditions**

| | | | |
|---|---|---|---|
| number of nozzle guide vanes | 24 | rotor tip clearance / span [%] | 1.4 |
| number of rotor blades | 36 | 2nd vane clearance / span [%] | 1.3 |
| number of 2nd guide vanes | 24 | 1st vane-blade spacing [% nozzle axial chord (midspan)] | 47 |
| nozzle chord (midspan) [mm] | 78.9 | blade-2nd vane spacing [% blade axial chord (midspan)] | 73 |
| nozzle axial chord (midspan) [mm] | 56.1 | pressure ratio $p_{tA}/p_C$ | 3.30 |
| geometric turning angle nozzle [°] | 70 | pressure ratio $p_{tA}/p_D$ | 4.27 |
| nozzle aspect ratio (exit height / chord) | 0.70 | rotational speed [rpm] | 10600 |
| blade chord (midspan) [mm] | 55.9 | inlet total temperature $T_{tA}$ [K] | 413 |
| blade axial chord (midspan) [mm] | 46.8 | Reynolds number nozzle guide vane exit | $2.57\ 10^6$ |
| geometric turning angle blade [°] | 107 | Reynolds number rotor blade exit | $1.69\ 10^6$ |
| blade aspect ratio (exit height / chord) | 1.24 | isentropic 1st vane exit Mach number | 1.13 |
| 2nd vane chord (midspan) [mm] | 88.3 | blade outlet Mach number, midspan | 0.51 |
| 2nd vane axial chord (midspan) [mm] | 80.1 | relative blade outlet Mach number, midspan | 0.87 |
| geometric turning angle 2nd vane [°] | 53 | 2nd vane outlet Mach number | 0.69 |
| 2nd vane aspect ratio (exit height / hord) | 0.88 | loading factor $\Delta h/u^2$ | 1.51 |

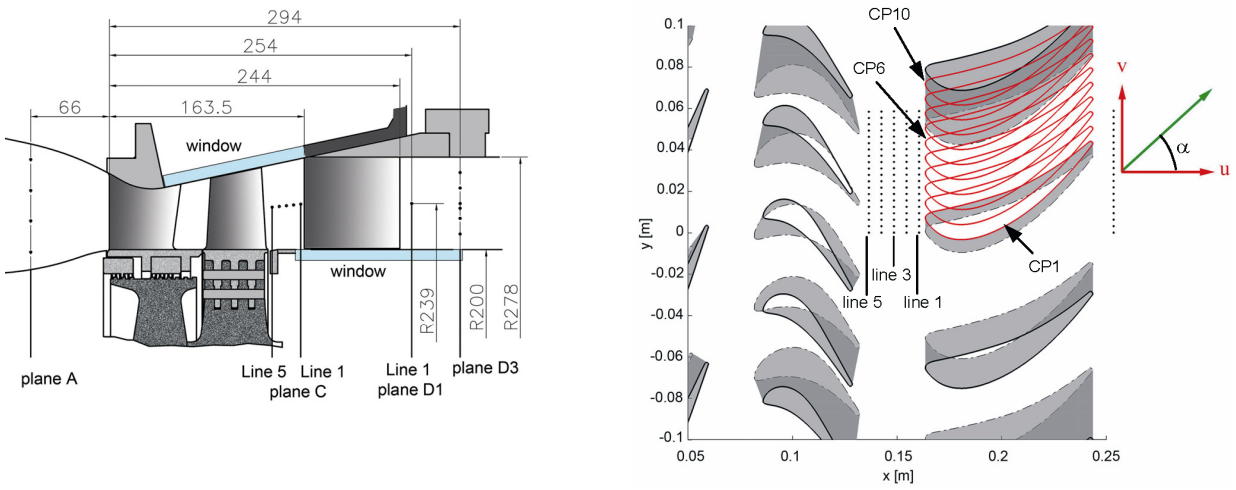


**Fig. 1: Meridional flow path (left) and investigated clocking positions with LDV-measurement locations (right)**

All circumferential LDV-measurements for each clocking position were performed by turning both vane rows, while the probe volume remained in a fixed position. By varying the angular position of the second vane row relative to the first vane row different clocking positions were investigated. Altogether the measurements were performed for ten different clocking positions downstream of the second vane row and two different clocking positions upstream of the 2nd vane row.

Figure 1 shows the investigated clocking positions as well as the LDV measurement locations upstream and downstream of the second vane row. Each circumferential line consists of 20 measurement positions and covers one vane pitch. To investigate the upstream influence of the second vane row, five circumferential lines were measured in plane C with an axial spacing of 6 mm. The measurement line 1 is located 3 mm upstream of the leading edge of the second vane.

Since a two-component LDV was applied, only the velocities in two different directions (i.e. axial and circumferential direction) were detected. In each measurement position approximately 80,000 velocity bursts were collected. These samples were sorted with the help of the trigger signal provided by the shaft monitoring system to the proper rotor position. All data recorded were then mapped into one 10° section, i.e. into one blade passing period (time for one rotor blade to move over one rotor pitch). As a result the data represent the average value over 36 rotor blade channels.

The blade passing period was divided into 40 evaluation windows, which means that the averaged velocity samples were assigned to 40 different first vane-rotor positions per rotor blade pitch. The instantaneous velocity data were ensemble averaged for each evaluation window. A linear regression method presented in Glas et al. (2000) was used. The instantaneous velocity vector **V** was decomposed as follows:

$$\mathbf{V} = \overline{\mathbf{V}} + \mathbf{V}' = \overline{\overline{\mathbf{V}}} + \widetilde{\mathbf{V}} + \mathbf{V}' \tag{1}$$

The last term **V'** represents an unresolved fluctuating component after ensemble averaging and may contain coherent structures that are not a harmonic of blade passing. Here it is used to quantify the level of turbulence in each evaluation window by means of the variance. With 40 evaluation windows the number of velocity samples per window was still high enough to allow mean value and level of turbulence to be calculated with the data presented in Tab. 3. With a circumferential averaged velocity of 245 m/s in plane D1 and 165 m/s in plane C (line 1) and a confidence level of 95% following errors for the ensemble averaged velocity and the unresolved fluctuation velocity are expected:

**Table 3: LDV measurement uncertainties**

| measurement position | $\overline{u}$ , $\overline{v}$ [%] | $u'$ , $v'$ [%] |
|---|---|---|
| inside the 2nd vane row | +/-1.6 | +/-5.5 |
| outside the 2nd vane row | +/- 0.7 | +/-2.3 |
| inside the rotor wake | +/- 1.7 | +/-6 |
| outside the rotor wake | +/- 0.4 | +/- 1.5 |

The high velocity uncertainty in the wake is due to the low number of detected velocity bursts in the wake (the shedding boundary layer contains less seeding particles).

## UNSTEADY THREE-DIMENSIONAL NAVIER-STOKES SIMULATION

The computations were performed using the in-house Navier-Stokes code LINARS, developed at Graz University of Technology (Pecnik et al., 2003, Pecnik et al., 2005, Pecnik and Sanz, 2006).

The compressible Reynolds/Favre-averaged Navier-Stokes (RANS) equations are solved in conservative form by means of a fully-implicit time-marching finite-volume method on structured curvilinear grids in multiblock alignment. The inviscid (Euler) fluxes are discretized with the upwind flux-difference splitting method of Roe (1981). In order to achieve a high order of spatial

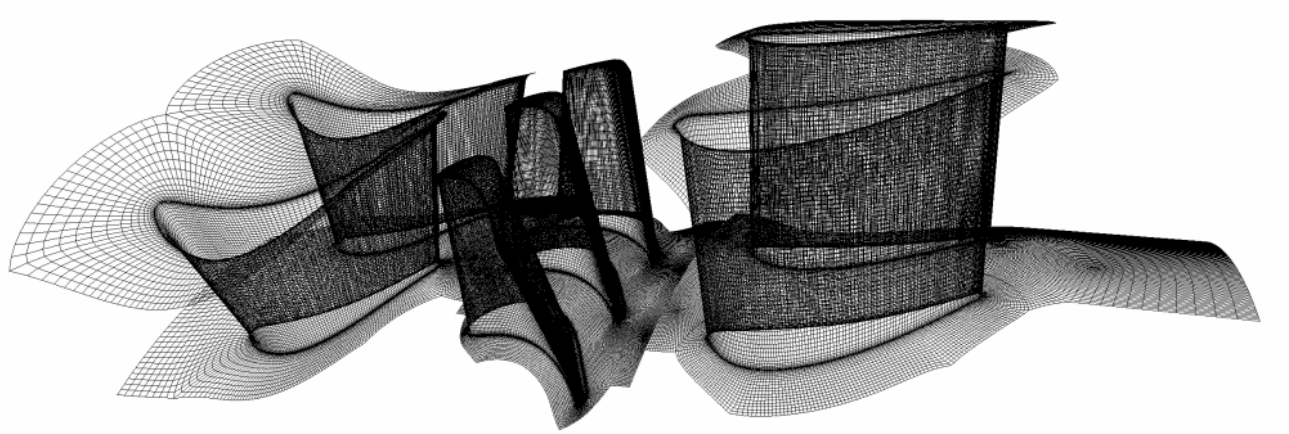

**Fig. 2: Computational domain. The picture shows the surface mesh of the computational grid used for CFD. The fillets between blade-hub and blade-outer casing and the rotor blade clearance are meshed to match the geometrical details of the test turbine facility**

accuracy a total variation diminishing (TVD) scheme with third-order interpolation was applied to get the state vector at each cell interface. The viscid flux vector at the cell interfaces is constructed with a second-order accurate central-differencing scheme using Green's theorem. To obtain a linear set of the time dependent Navier-Stokes equations a second order accurate Newton-Raphson procedure is applied for the discretization in time. At the left-hand side of the equation system the inviscid fluxes are treated with first order accuracy and the viscid fluxes with a thin-layer approximation to obtain a block-tri-diagonal matrix for each grid index line. This linear equation set is solved by the alternating direction implicit (ADI) scheme.

To cope with unequal pitch ratios, the code uses phase-lagged boundary conditions by means of a direct store technique at geometrical periodic boundaries and hence only one passage each blade row was simulated with a total of app. 2,000,000 cells. In this work one blade passing period was calculated with 480 time steps for the rotor and 320 time steps for both stator passages. Furthermore to save computational time and memory pressure gradient wall-functions based on the law-of-the-wall formulation by Spalding were used (Pieringer and Sanz, 2005). The turbulence was calculated using the one equation turbulence model of Spalart and Allmaras (1994).

The geometrical details of the turbine stage containing the fillets and the rotor tip clearance are modeled as well (see Fig. 2). The clearance of the second vane to the hub was not modeled.

In Fig. 3 the visualization was done with an in-house post-processing tool, where the instantaneous flow field was discussed by means of the magnitude of the pressure gradient and the radial vorticity.

## RESULTS AND DISCUSSION

### Vane-Rotor-Vane interaction mechanism

The high-pressure ratio of the investigated turbine stage causes a pronounced shock system, especially at the nozzle guide vane outlet. Considerable insight into the flow-field is obtained from the numerical simulation. The upper plot of Fig. 3 presents contour plots of the radial vorticity and isolines of the pressure-gradient-magnitude for CP1 at midspan. Eight frames are shown corresponding to one blade passing period $\tau$. Due to a vane blade ratio of 2:3 the same instantaneous flow-field is observed between two neighboring vanes with a time delay of 50% (e.g. Fig. 3, $t/\tau=0$ and $t/\tau=0.5$).

At $t/\tau=0.5$ the suction side trailing edge shock of the nozzle guide vane impinges the suction side of the rotor blade "1". At $t/\tau=0.625$ the reflected shock "A" moves upstream and at

approximately $t/\tau=0.875$ the shock wave reaches the pressure side of blade "2" and is reflected again towards the blade's suction side (marked with "B").

The reflected shock "A" propagates upstream ($t/\tau=0$ to $t/\tau=0.5$) and interferes destructivly with a previously shock wave "A" at approximately to $t/\tau=0.5$. Hence, a part of the reflected shock "A" impinges weakly on the suction side of the nozzle guide vane "1" at $t/\tau=0.5$ and enforces a vortex separation. From then on the vortex shedding is undisturbed, until the next reflected shock wave triggers again. This shock wave induced phase locking phenomena which were explained in detail by Göttlich et al. (2006).

The other part of the shock wave "A" impinges more strongly at the suction side of the nozzle guide vane "2" (not shown in Fig. 3, or rather at vane "24" at $t/\tau=0.75$) and is reflected again ($t/\tau=0.875$, marked with "C"). The shock wave "C" propagates downstream ($t/\tau=0$ to $t/\tau=0.25$) and interacts first with the shock wave "B" at $t/\tau=0.375$ and interacts afterwards with the trailing edge shocks at approximately $t/\tau=0.75$. The resulting shock wave marked with "D" propagates downstream and impinges the leading edge of the second vane for CP1 ($t/\tau=0.25$).

A modulation of the rotor's trailing edge shocks with respect to the circumferential position is clearly visible in Fig. 3. At axial positions where the rotor wakes and the suction side trailing edge shocks "E" interact a shock weakening is observed. Hummel (2002) explained this by a splitting of the shocks due to vane wake induced shock motions in the relative frame of reference. The author suggested positioning a second vane at this axial distance to reduce the impact of the shocks onto the leading edge. Since Hummel (2002) investigated a single stage turbine the influence of a second vane onto the shock strength was not discussed. In this work the second stator is positioned at the axial distance where the rotor trailing edge shock interacts with the following rotor wake.

The suction side trailing edge shocks "E" impinges weakly at the suction side of the second vane and sweeps towards the leading edge of the second vane.

In Fig. 3 vorticity contour plots are used to identify the nozzle guide vane wakes as well as the rotor wakes. The nozzle guide vane vortex street is chopped by the rotor and is then convected through the rotor passage (details of wake-blade interactions are given by Hodson and Dawes, 1998). The counter-rotating nozzle wake parts are still visible in the rotor exit flow and modulate the strength of the shedding vortices (Hummel, 2002, Göttlich et al., 2006). At CP1 these wake segments convect between two vanes, whereas at CP6 the first vane wakes impinge the leading edge of the second vane (see Fig. 3, $t/\tau=0$, encircled region).

*Effect of Clocking onto the shock wave propagation*

The flow-field of the opposite clocking position (CP6) is given at the bottom of Fig. 3. The interaction of the induced static pressure field of the second vane with the total pressure field at rotor exit (mainly induced by the nozzle guide vane) has a minor effect on the trailing edge shocks close to the rotor exit. Miller et al. (2003b) performed time resolved rotor surface-pressure measurements in a transonic turbine stage. The authors found that clocking only affects the rear part of the rotor suction side (downstream the geometric throat). Therefore, upstream of the pressure side trailing edge shock the instantaneous flow-field of both clocking positions is identical.

At CP6 the suction side trailing edge shocks close to the second stator is hardly diminished as a result of the favorable interaction of the total pressure field at rotor exit and the potential field of the second vane. As previously discussed the pressure wave ("D") propagates between two vanes for CP6. Therefore at CP6 the second vane boundary layer is less disturbed by shock waves.

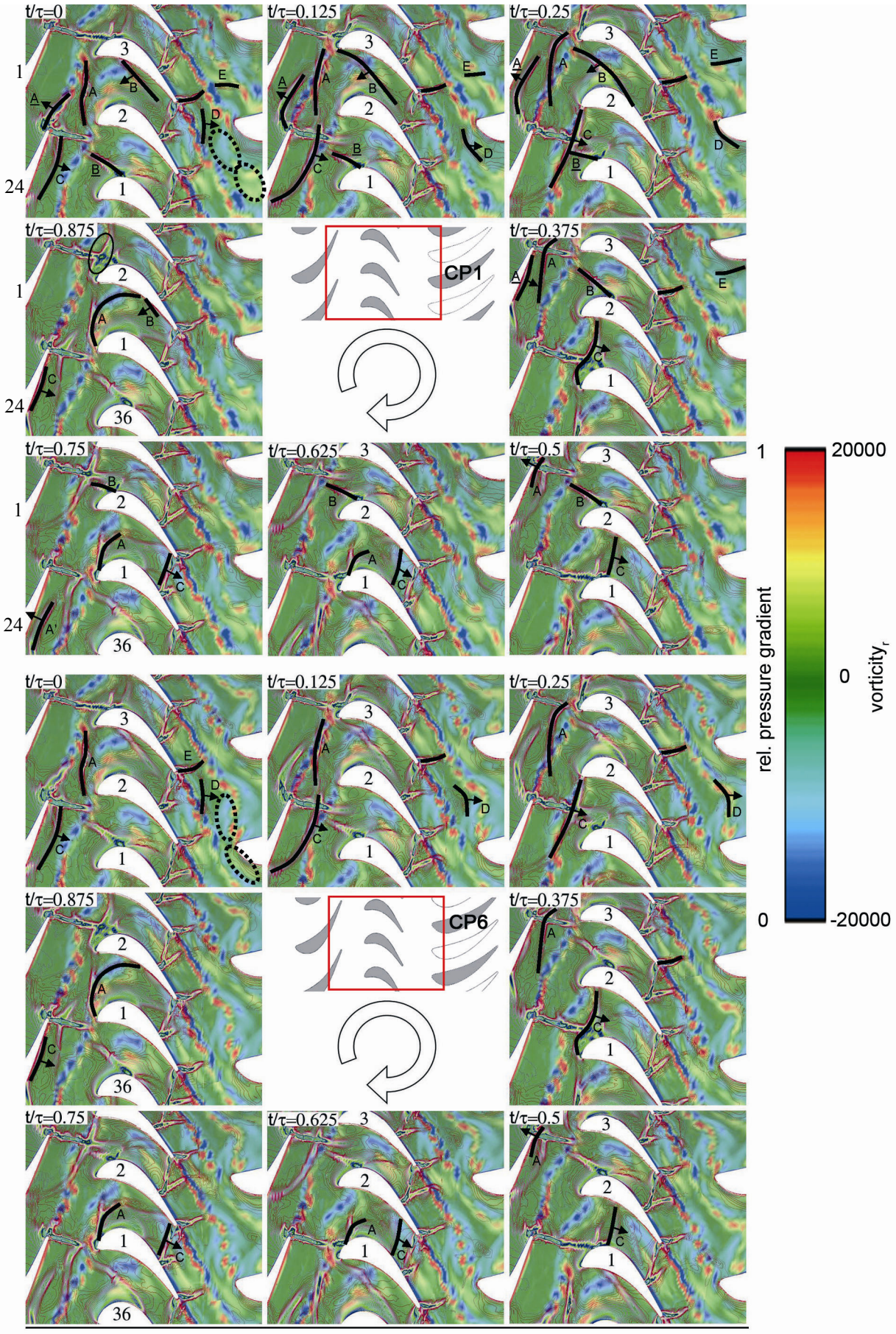


**Fig. 3: Contour plot of radial vorticity and isolines of pressure gradient magnitude for CP1 (top) and CP6 (bottom) obtained by CFD**

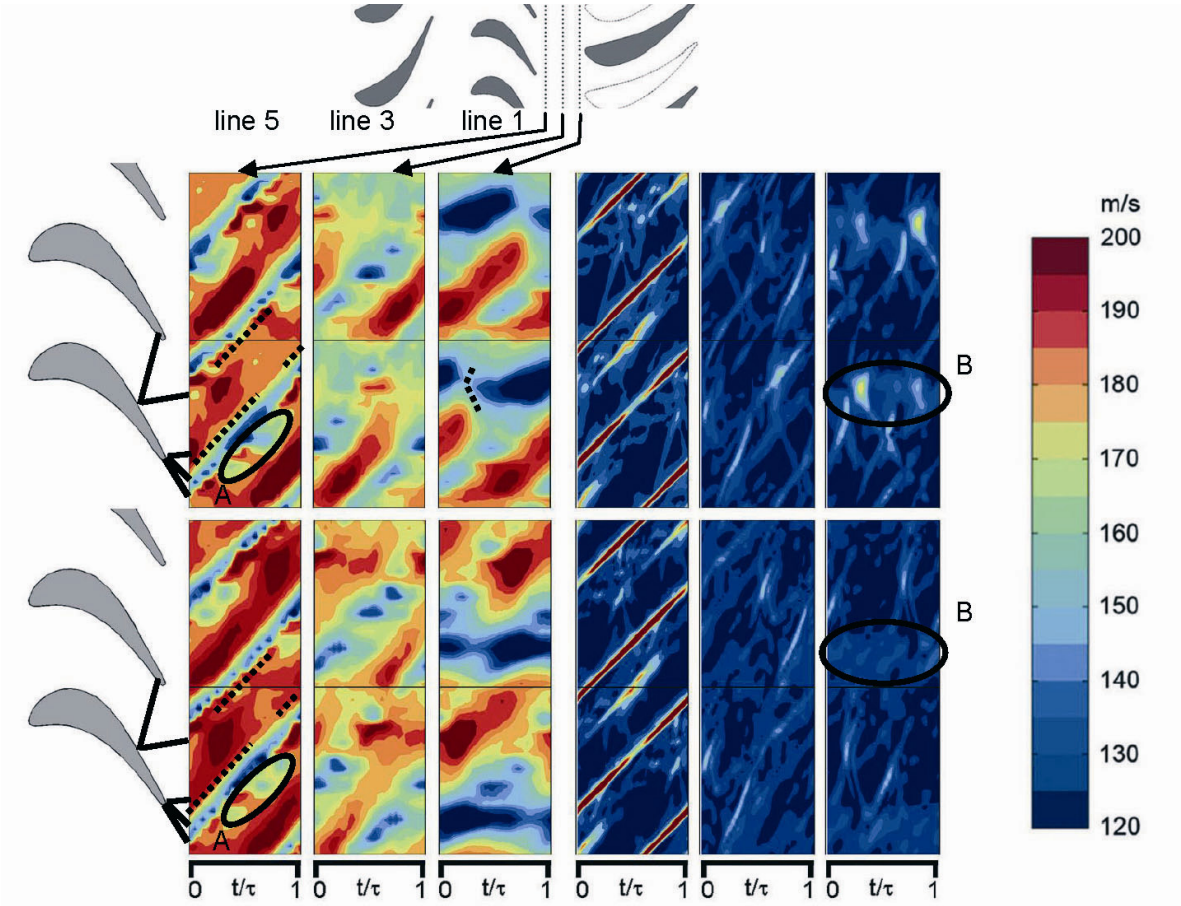


**Fig. 4: Left plots: Time-space plots of velocity magnitude for CP1 (upper plots) and CP6 gained by LDV; Right plots: Time-space plots of pressure gradient for CP1 (upper plots) and CP6 gained by CFD**

*Time resolved Laser-Doppler-Velocimetry results*

Downstream of the rotor three LDV-measurement lines are discussed to validate the prediction. Time-space plots are a suitable tool to visualize these instantaneous data. Due to the dimensions used in the data presentations, structures from the moving rotor trailing edge appear under an angle of 45°, where effects from the vanes are horizontal contours. Figure 4 presents time-space plots of the velocity magnitude for CP1 and CP6 as well as time-space plots of the pressure gradient obtained by CFD. The plots are dominated by the rotor wakes, the periodic first vane wake passing "A" and the trailing edge shocks. The dotted lines parallel to the rotor wake mark the reflected pressure side shocks and the suction side shocks. A horizontal modulation of the shock strength can be observed. Close to the rotor exit the circumferential position of this modulation is not affected by different clocking positions. This is an indication that the nozzle guide vane causes this modulation.

The interaction of the total pressure field (mainly imposed by the nozzle guide vane) at the rotor exit with the potential field of the second vane becomes stronger at measurement line 3. The shock strength changes for different clocking positions. This can be seen easily in the time-space plots of the pressure gradient. The region of low velocity seen in measurement line 1 (close to the second vane row) identifies the circumferential position of the vane's leading edge. The time periodic impingement of the rotor wakes on the leading edge of the second vane cause distinct maxima and minima in the velocity magnitude. These maxima are more pronounced at CP1 than at CP6.

Furthermore, higher shock strength can be detected for CP1 as previous discussed in Fig. 3, indicated with "B" in Fig. 4. This strong shock wave could form a boundary layer separation bubble resulting in higher loss within and downstream of the bubble (Denton, 1993).

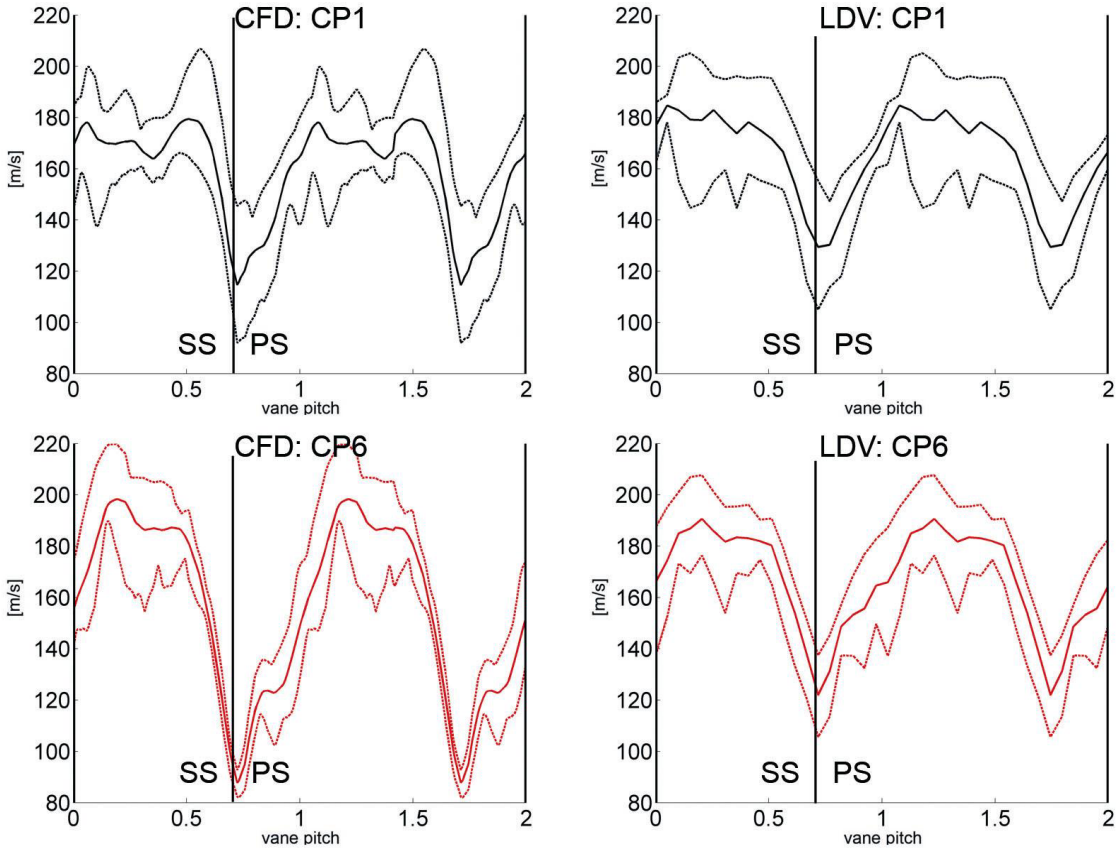


**Fig. 5: Comparison of CFD (left) and LDV (right): Time-averaged and maximum-minimum envelope of the velocity magnitude for CP1 (top) and CP6 (bottom); plane C, Line 1: 3 mm upstream the second vane**

### Clocking mechanism

Figure 5 presents the time-averaged velocity and the maximum-minimum envelopes at measurement line 1 (close to the second vane leading edge) for both clocking positions. In Fig. 5 CP6 is shifted in that sense that the second vane leading edge remains at a fixed position. At CP6 the nozzle guide vane wake impinges the second vane's leading edge. Close to the leading edge a velocity decrease of 23% is predicted, while with LDV a velocity decrease of only 6% is observed for CP6 (note that the velocity amplitude decreases by 11%, Schennach et al., 2006). Furthermore, the difference between maximum and minimum envelope is less pronounced close to the leading edge, which is a result of the time periodic first vane wake passing (see also Fig. 4). Griffin et al. (1996) found that reduced surface velocities and less large-scale unsteadiness are the reasons for the improved second vane performance.

The overall agreement between prediction and measurement is satisfying. The use of the Spalart and Allmaras turbulence model results in lower wake mixing effects and thus lower wake velocities are predicted. Furthermore, at the circumferential positions where the first vane wake passes through the largest deviation between CFD and LDV is observed.

*Second vane wall shear stress*

Figure 6 presents the time averaged as well as the maximum and minimum envelope of the wall shear stress for both clocking positions. Overall CP6 shows lower wall shear stress values (except in the rear part of the suction side), which results in less entropy creation in the boundary layer. Moreover at the axial distance $x/l_{ax}$=0.15 large fluctuations on the suction side are observed for CP1.

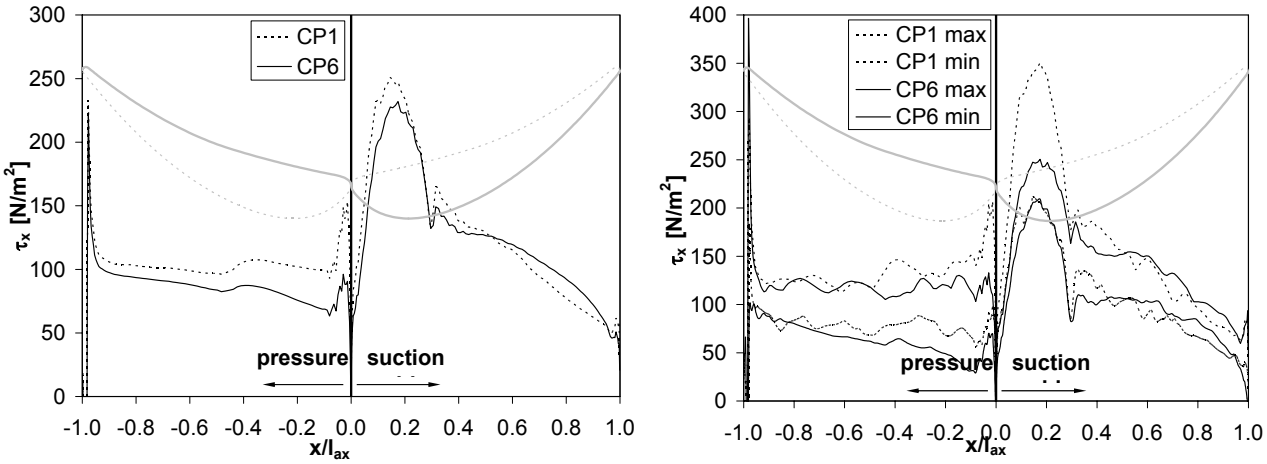


**Fig. 6: Left plot: wall shear stress distribution at the second vane for CP1 and CP6; right plot: maximum and minimum envelope of wall shear stress**

*Flow downstream the second stator*

The time-averaged velocity magnitude and the velocity envelopes for both clocking positions are shown in Fig. 7. The prediction and the measurements indicate a significant increase of the second vane wake depth for CP6. Besides the wakes the overall agreement between prediction and measurement is satisfying. In contrast to Fig. 5 the prediction shows higher velocities in the wake. It is believed that the "hub leakage flow" (not modeled in the CFD calculation) and a periodic boundary layer separation causes this difference. This could also explain the large unsteadiness in the second vane wake observed in the measurements.

Schennach et al. (2006) examined the spanwise total-to-total efficiency variation due to clocking using a total pressure and a total temperature rake at outlet for five different spans. A +/- 1.6 % variation near midspan for CP6 was found providing the highest efficiency at midspan. Due to the cylindrical second vane design the optimum clocking position varies over the height, with the lowest influence on efficiency at the tip.

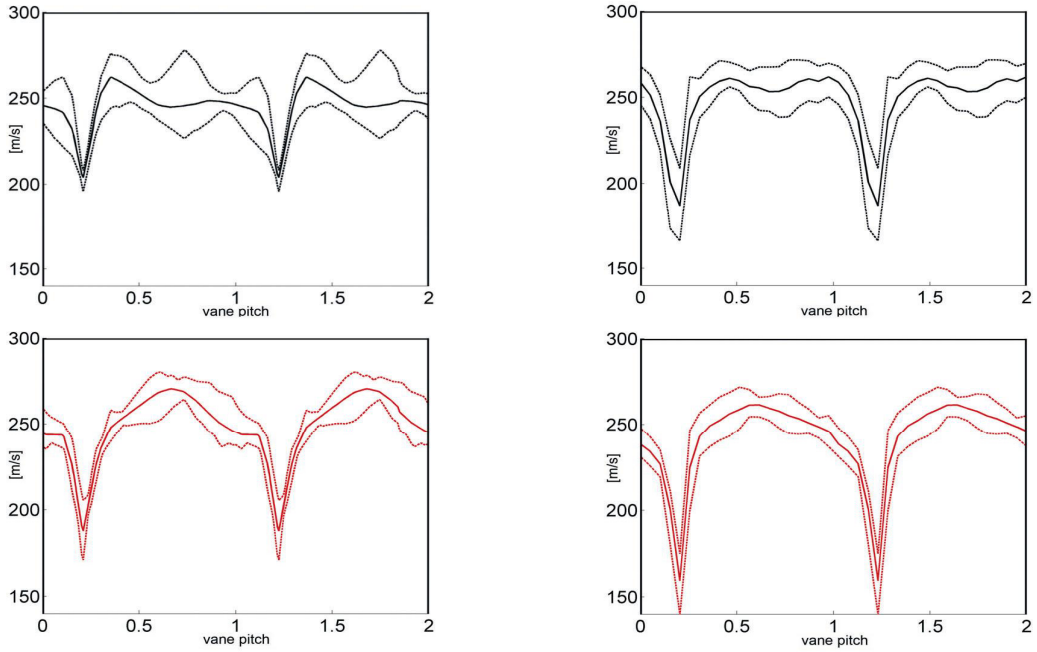


**Fig. 7: Comparison of CFD (left) and LDV (right) : Time-averaged velocity magnitude and maximum-minimum envelope of the velocity magnitude for CP1 (top) and CP6 (bottom); plane D, Line 1: 10 mm downstream of the second vane**

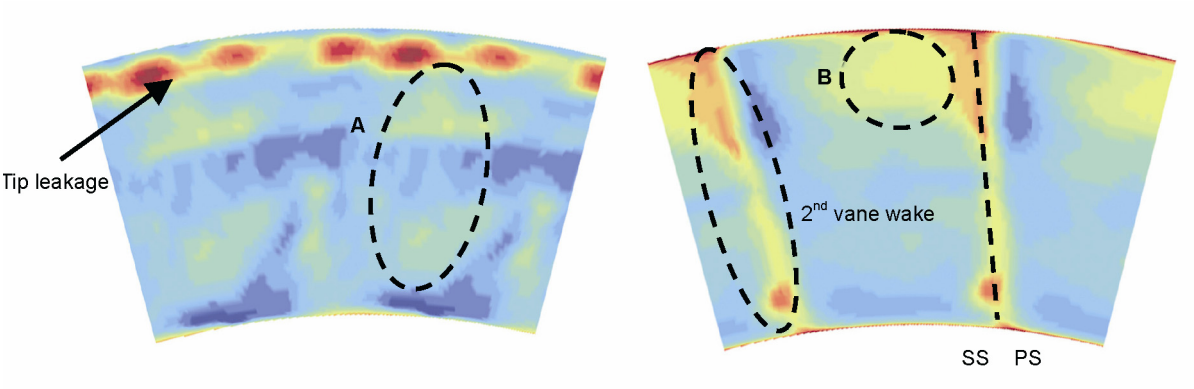


**Fig. 8: Time-averaged contour plot of entropy for CP1; plane C1 (left) and plane D1 (right), red color indicates high entropy values**

Figure 8 presents time averaged contour plots of entropy for CP1 upstream and downstream of the second vane. The main structure in plane C1 is the strong tip leakage flow, with a pronounced modulation in circumferential direction. Regions with higher entropy over the span indicate the losses linked with the nozzle guide vane (marked with "A"). Downstream of the second vane close to the tip a loss core is apparent which is evoked from the rotor tip leakage flow and the upper passage vortex of the second vane.

These results show that the secondary flow field has a major influence on the clocking phenomena in a low aspect ratio turbine. Future work is necessary to discuss the three dimensional flow and the clocking effect on the secondary flows.

## CONCLUSIONS

In the presented paper vane clocking in a 1.5 stage transonic turbine was investigated using Laser-Doppler-Velocimetry and an unsteady three-dimensional Navier-Stokes simulation. Two selected clocking positions were discussed in detail with special focus onto the midspan. The prediction was compared with the LDV results and showed good overall agreement.

A detailed discussion of the shock interaction mechanism with respect to clocking was given. It was found that clocking has a minor influence onto the trailing edge shocks close to the rotor exit. While in low-pressure turbines the dominant clocking mechanisms are the wake trajectories, in transonic turbines additionally shock waves must be taken into account. In the clocking position where the first vane wake impinges the leading edge of the second vane a lower velocity-magnitude close to the leading edge of the second vane was observed. This results in lower wall shear stress of the second vane and thus in less entropy production. Furthermore a decreased shock strength close to the leading edge was found for the same clocking position.

## ACKNOWLEDGEMENTS

This work was made possible by the Austrian Science Fund (FWF) within the grant P16521-N07 "Experimental Investigation of the Stator-Rotor-Stator Interaction in a Transonic Turbine". The support of Dr. H. P. Pirker in the operation of the compressor station is also gratefully acknowledged.

## REFERENCES

Arnone, A., Marconcini, M., Pacciani, R., Schipani, C., and Spano, E., 2002, "Numerical Investigation of Airfoil Clocking in a Three-Stage Low-Pressure Turbine," ASME J.Turbomach.,**124**(1), pp. 61-68.

Billiard, N., Paniagua, G., and Dénos, R., 2005, "Effect of Clocking on the Heat Transfer Distribution of a Second Stator Tested in a One and a Half Stage HP Turbine," ASME Paper No. 2005-GT-68462.

Denton, J. D., 1993, "Loss Mechanisms in Turbomachines," ASME J. Turbomach., **115**(4), pp. 621-656.

Erhard, J., and Gehrer, A., 2000, "Design and Construction of a Transonic Test Turbine Facility," ASME Paper No. 2000-GT-480.

Gadea, J., Dénos, R., Paniagua, G., Billiard, N., and Sieverding, C. H., 2004, "Effect of Clocking on the Second Stator Pressure Field of a One and a Half Stage Transonic Turbine," ASME Paper No. 2004-GT-53463.

Glas, W., Forstner, M., Kuhn, K., and Jaberg, H., 2000, "Smoothing and Statistical Evaluation of LDV Data of Turbulent Flows in Reciprocating Machinery," Experiments in Fluids, **29**, pp. 411-417.

Göttlich, E., Woisetschläger, J., Pieringer, P., Hampel, B., and Heitmeir, F., 2005, "Investigation of Vortex Shedding and Wake-Wake Interaction in a Transonic Turbine Stage Using Laser-Doppler-Velocimetrie and Particle-Image-Velocimetrie," ASME J. Turbomach., **128**(1), pp. 178-187.

Griffin, L. W., Huber, F. W., and Sharma, O. P., 1996, "Performance Improvement Through Indexing of Turbine Airfoils: Part 2-Numerical Simulation," ASME J. Turbomach., **118**(4), pp. 636-642.

Haldeman, C. W., Dunn, M. G., Barter, J. W., Green, B. R., and Bergholz, R. F., 2004, "Experimental Investigation of Vane Clocking in a One and ½ Stage High Pressure Turbine," ASME Paper No. 2004-GT-53477.

Huber, F. W., Johnson, P. D., Sharma, O. P., Staubach, J. B., and Gaddis, S. W., 1996, "Performance Improvement Through Indexing of Turbine Airfoils: Part 1-Experimental Investigation," ASME J. Turbomach., **118**(4), pp. 630-635.

Hummel, F., 2002, "Wake-Wake Interaction and Its Potential for Clocking in a Transonic High-Pressure Turbine," ASME J. Turbomach., **124**(1), pp. 69-76.

Hodson, H. P., Dawes, W. N., 1998, "On the Interpretation of Measured Profile Losses in Unsteady Wake-Turbine Blade Interaction Studies," ASME J. Turbomach., **120**(2), pp. 276-284.

König, S., Heidecke, A., Stoffel, B., Fiala, A., and Engel, K., 2004, "Clocking Effects in a 1.5-Stage Axial Turbine – Boundary Layer Behaviour at Midspan," ASME Paper No. 2004-GT-54055.

Miller, R. J., Moss, R. W., Ainsworth, R. W., and Horwood, C. K., 2003a, "Time-Resolved Vane-Rotor Interaction in a High-Pressure Turbine Stage," ASME J. Turbomach., **125**(1), pp. 1-13.

Miller, R. J., Moss, R. W., Ainsworth, R. W., and Harvey, N. W., 2003b, "Wake, Shock, and Potential Field Interactions in a 1.5 Stage Turbine-Part I: Vane-Rotor and Rotor-Vane Interaction," ASME J. Turbomach., **125**(1), pp. 33-39.

Neumayer, F., Kulhanek, G., Pirker, H. P., Jericha, H., Seyr, A., and Sanz, W., 2001, "Operational Behavior of a Complex Transonic Test Turbine Facility," ASME Paper No. 2001-GT-489.

Pecnik, R., Pieringer, P., Sanz, W., 2004, "Numerical Investigation of the Secondary flow of a Transonic Turbine Stage Using Various Turbulence Closures", GT2005-68754, Proceedings of ASME Turbo Expo 2005, June 6-9, 2005, Reno-Tahoe, Nevada, USA

Pecnik, R., Sanz, W., Gehrer, A., Woisetschläger, J., 2003, "Transition Modeling using Two Different Intermittency Transport Equations", J. Flow, Turbulence and Combustion 70, 299-323

Pecnik, R., Sanz, W., 2006, "Application of the Turbulent Potential Model to Heat Transfer Predictions on a Turbine Guide Vane", Proceedings of ASME Turbo Expo 2006, May 8-11, 2006, Barcelona, Spain

Pieringer P., Sanz W., 2005, "A Pressure Gradient Sensitive Wall Function for the Prediction of Turbulent Flow in Thermal Turbomachinery", GT2005-68471, Proceedings of ASME Turbo Expo 2005, June 6-9, 2005, Reno-Tahoe, Nevada, USA

Reinmöller, U., Stephan, B., Schmidt, S., and Niehuis, R., 2002, “Clocking Effects in a 1.5 Stage Axial Turbine-Steady and Unsteady Experimental Investigations Supported by Numerical Simulations,” ASME J. Turbomach., **124**(1), pp. 52-60.

Roe P.L., 1981, “Approximate Riemann Solvers, Parameter Vectors and Differencing Scheme”, Journal of Computational Physics 43, 357-372

Tiedemann, M., and Kost, F., 2001, “Some Aspects of Wake-Wake Interactions Regarding Turbine Stator Clocking,” ASME J. Turbomach., **123**(3), pp. 526-533.

Schennach, O., Woisetschläger, J., Fuchs, A., Göttlich, E., Marn, A., and Pecnik, R., 2006, “Experimental investigations of clocking in a one and a half stage transonic turbine using Laser-Doppler-Velocimetry and a fast response aerodynamics pressure probe ASME Paper No. 2006-GT-90264, accepted for the *ASME J Turbomachinery.*

Spalart, P.R., Allmaras S.R., 1994 “A One Equation Turbulence Model for Aerodynamic Flows”, La Recherche Aerospatiale, No.1, pp. 5-21